Electrotaxis evokes directional separation of co-cultured keratinocytes and fibroblasts

scientific reports

Check for updates

OPEN

Electrotaxis evokes directional separation of co-cultured keratinocytes and fibroblasts

José Leal[1,2,6]✉, Sebastian Shaner[1,2,6], Nicole Jedrusik[1,2], Anna Savelyeva[1,2] & Maria Asplund[1,2,3,4,5]✉

Bioelectric communication plays a significant role in several cellular processes and biological mechanisms, such as division, differentiation, migration, cancer metastasis, and wound healing. Ion flow across cellular walls leads to potential gradients and subsequent formation of constant or time-varying electric fields(EFs), which regulate cellular processes. An EF is natively generated towards the wound center during epithelial wound healing, aiming to align and guide cell migration, particularly of macrophages, fibroblasts, and keratinocytes. While this phenomenon, known as electrotaxis or galvanotaxis, has been extensively investigated across many cell types, it is typically explored one cell type at a time, which does not accurately represent cellular interactions during complex biological processes. Here we show the co-cultured electrotaxis of epidermal keratinocytes and dermal fibroblasts with a salt-bridgeless microfluidic approach for the first time. The electrotactic response of these cells was first assessed in mono-culture to establish a baseline, resulting in the characteristic cathodic migration for keratinocytes and anodic for fibroblasts. Both cell types retained their electrotactic properties in co-culture leading to clear cellular partition even in the presence of cellular collisions. The methods leveraged here pave the way for future co-culture electrotaxis experiments where the concurrent influence of cell types can be thoroughly investigated.

Bioelectricity plays a role in all mammalian somatic cells, not just excitable ones. The main bioelectric difference between excitable and non-excitable cells is the time scale: milliseconds for the former and minutes to days for the latter[1]. While action potentials are how information is relayed in excitable cells, non-excitable cells depend on gap junctions to pass bioelectric information to their neighbors. A canonical example is found within the epidermis during wound healing. A gradient of ions from the outermost layer (apical) to the innermost layer (basal) of the epidermis generates a transepithelial potential (TEP). When the skin and TEP are broken, a new ionic gradient is formed, with the current pointing toward the center of the newly-formed wound. This endogenous electric field (EF) is crucial in wound healing. It acts as a bioelectric beacon for nearly all cells responsible for cleanup, repair, and remodeling.

The directed migration of cells along or against an EF's direction is called electrotaxis or galvanotaxis. This phenomenon occurs throughout the body and plays a major role in wound healing[2], neuronal migration, and regeneration[3], bone maintenance[4], mesenchymal cell migration[5,6], and cancer invasion[7–15]. Electrotaxis has been extensively investigated in vitro in over 30 cell types (both non-excitable and excitable)[16,17]. Several biochemical mechanisms have been reported to be directly involved and responsible for electrotaxis: signaling pathways (e.g., phosphatidylinositol-3-OH kinase (P3IK), mitogen-activated protein kinase (MAPK))[18,19], voltage-gated ion channels (e.g., sodium- and calcium-selective)[20,21], and growth factors (e.g., epidermal, vascular endothelial)[22]. While these relate to specific cell types, more global bioelectric mechanisms have also been identified. The extracellular EFs impart asymmetrical mechanical intracellular forces, and sequential intracellular pathway activation cascades through spatial and polar redistribution of charged cell membrane receptors (e.g., ion channels, integrins) through electrophoretic or electroosmotic forces[23–26].

The interplay between bioelectric and biochemical driving factors during electrotaxis likely overlaps across cell types and species to varying degrees. The culmination of these factors gives rise to a direct electrotactic response.

[1]Department of Microsystems Engineering (IMTEK), University of Freiburg, Freiburg, Germany. [2]BrainLinks-BrainTools Center, University of Freiburg, Freiburg, Germany. [3]Freiburg Institute for Advanced Studies (FRIAS), University of Freiburg, Freiburg, Germany. [4]Department of Microtechnology and Nanoscience, Chalmers University of Technology, Gothenburg, Sweden. [5]Division of Nursing and Medical Technology, Luleå University of Technology, 97187 Luleå, Sweden. [6]These authors contributed equally: José Leal and Sebastian Shaner. ✉email: jose.leal@blbt.uni-freiburg.de; maria.asplund@chalmers.se

The vast majority of cells migrate toward the more negatively-charged electrode (i.e., cathode); however, some cell types migrate toward the anode[27]. This electrotactic phenotype duality is also a characteristic of the cells partaking in the wound-healing process. Dermal fibroblasts migrate anodically, while keratinocytes migrate cathodically. This differing electrotactic response for keratinocytes and fibroblasts has been shown in vitro to be strongly regulated by PI3K signaling. Furthermore, these cells show an electrotactic response at different EF strengths. Keratinocytes exhibit directed migration at 100 mV mm^{-1} after 1 h[28], while fibroblasts require either longer times (3 h at 100 mV mm^{-1}) or higher EFs (1 h at 400 mV mm^{-1})[18]. In vivo, these cells appear to migrate at different intervals during the proliferation and remodeling phases of wound healing while simultaneously influencing each other through diverse signaling pathways[29]. The keratinocyte-fibroblast interaction in wound healing is still not fully understood, particularly regarding the role of endogenous EFs in orchestrating migration. Developing a technological platform where these cells can be co-cultured and simultaneously stimulated can benefit the understanding of the interplay of previously known signals and EFs during wound healing[28,30,31].

To investigate how electrotaxis fundamentally works, one must recreate the biological endogenous driving force, meaning a constant EF over a defined time frame, and observe how these fields affect cellular mechanisms, morphology, metabolism, and movement. Microfluidic devices can provide precise setups for electrotaxis research by controlling the distribution and tuning of electric fields (EF) in cell-containing microchannels[32,33]. However, there are some challenges associated with cell seeding, such as restricted volume and low surface area[34]. A technique that allows spot-cast seeding into laser-cut microchannels with subsequent device assembly previously developed by our group is leveraged here to overcome these difficulties[35]. The electrodes employed for direct current stimulation (DCs), such as silver/silver chloride (Ag/AgCl) or platinum (Pt), can produce cytotoxic chemical products and require careful experimental design prior to experimentation (i.e., use of salt bridges)[36–41]. To address this issue, we previously developed salt-bridgeless systems, which rely on metal or carbon electrodes coated with a supercapacitive conducting polymer or hydrogel based on PEDOT:PSS, which we leverage in this work[42,43]. These electrodes have excellent biocompatibility and stable DCs capabilities with cultured cells, as they mainly rely on ions available in the media (Na^+, K^+, Ca^{2+}, Cl^-) for charge delivery. Careful control of electrode and coating geometries, as well as the magnitude and duration of stimulation, help prevent the onset of unwanted Faradaic reactions (e.g., hydrolysis, corrosion). In our previous work, we measured pH changes at the media reservoirs during stimulation and concluded that slight pH changes happen close to the electrode but do not reach the cells within the microfluidic channel[35]. By thorough characterization, we have also identified safe operation windows where the electrodes remain in their pseudo-capacitive and biocompatible charge delivery mode[35,42,44]. This novel approach provides a streamlined alternative for faster in vitro electrotaxis experimentation with the potential for future in vivo applications[42,44].

In this study, we combine these technological developments to address two questions: **(1)** Will mono-cultured keratinocytes and fibroblasts stimulated in salt-bridgeless microfluidic devices electrotactically concur with findings using conventional salt-bridge systems? **(2)** Will co-cultured keratinocytes and fibroblasts exhibit the same electrotactic behavior as their mono-cultured counterparts? (Fig. 1) Until now, electrotaxis research on these cells has typically been conducted in buffered systems (i.e., using salt bridges), with a clear focus on understanding the underlying biological mechanisms governing electrotaxis (c.f. supplementary table ST1 and ST2). On the opposite side of the spectrum, wound healing therapy relying on electrical stimulation is typically conducted on the assumption that the employed electrodes and stimulation paradigms will elicit the desired cellular reaction without damage to the underlying tissue. A clear gap exists between fundamental research and

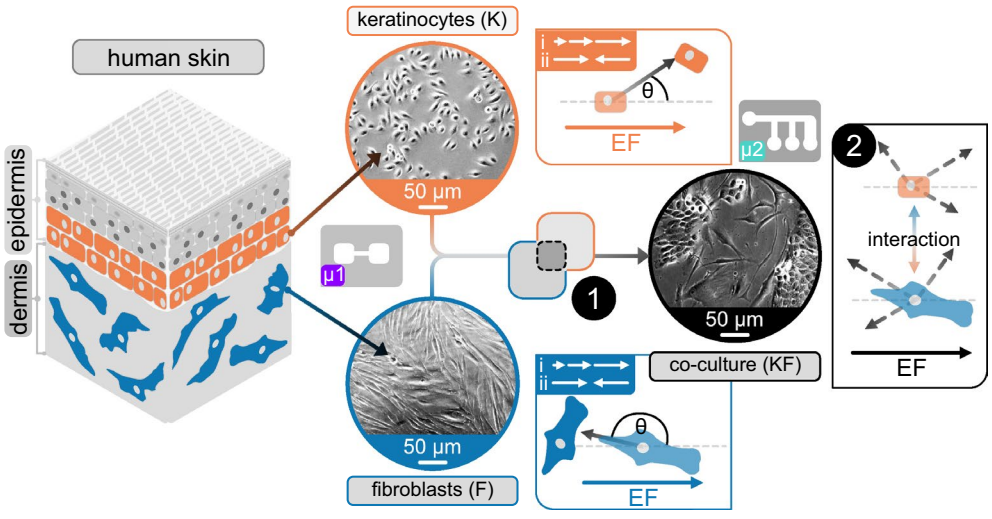

Figure 1. Visual representation of hypothesis. Keratinocytes and fibroblasts reside in different skin layers. Characterization of their electrotactic response for (**i**) different EF magnitudes and (**ii**) alternating EF directions is done in mono-culture (device µ1) and is compared to literature values. Co-culturing these cells requires adequate mixing and appropriate cell media to investigate if (**1**) these cells can be co-cultured and electrically stimulated and (**2**) if these cells show the same electrotactic behavior in mono- and co-culture.

clinical applications where electrotaxis is leveraged. More data is needed to develop adequate devices capable of exploiting this biological effect as a therapeutic approach. The first question of this work focuses on validating the cellular response of the two principal cells targeted in electrical wound healing therapy to the direct application of DCs with a novel electrode material. The second question aims at the development of a suitable platform to investigate the keratinocytes-fibroblast interaction during wound healing and the concurrent validation of their response to the simultaneous application of an EF. By evaluating the electrotactic response of these cells individually and in co-culture, one can develop therapeutic thresholds for EF dosages needed to test the effectiveness of future clinical electroceutical devices. Thus, allowing better control of the epidermal and dermal reconstruction of the wound bed[45].

For the first time, we demonstrate the concurrent electrotactic stimulation of co-cultured keratinocytes and fibroblasts. We present here two different microfluidic electrotaxis platforms to explore DC stimulation of human skin cells using salt-bridgeless electrodes in mono- and co-culture configurations. The first platform leverages soft lithography to yield consistent structures that individually enable electric field dosage dependency exploration of human keratinocytes and fibroblasts. This device allowed the initial determination of electrotactic thresholds as well as the influence of electrical polarity switching on cellular directionality dynamics in monocultures. The second platform exploits a double-sided adhesive to permit straightforward co-culture seeding and cultivation while having a current divider design that provides six different EF intensities from a single pair of electrodes. This platform leverages larger supercapacitive electrodes to achieve DC stimulation for many hours and assess the concurrent dynamics of keratinocyte and fibroblast electrotaxis. The combination of both bioelectronic microfluidic platforms enables direct comparison of electrotactic metrics of both cell types when they are alone or coupled.

Results

Mono-culture electrotaxis on human skin cells. *Keratinocytes migrate toward the cathode.* Both keratinocytes and fibroblasts were subjected to a step-wise increased EF magnitude to determine their threshold for electrotaxis. Figure 2 depicts cell migration for keratinocytes and Fig. 3 for fibroblasts under the influence of an externally applied EF field within a single-channel microfluidic device (***µ1***). Manual cell tracking during time-lapse imaging provides insight into individual cell movement dynamics, showcased in hairline plots for cells in a non-stimulated state (control) and under an external stimulus (Figs. 2A and 3A). The individual cells are then analyzed collectively to determine their directedness in relation to the applied EF (**+1** being toward the **cathode**, **-1** toward the **anode,** c.f., section "Live-cell imaging and direct current stimulation") and velocity. No adverse cellular reactions to the applied currents (i.e., cell death, impaired migration) were observed, indicating that electrical stimulation with a salt-bridgeless system is appropriate for the parameters and conditions applied here. For both cell types, the non-stimulated control showed random, non-directed movement, as is also expected in their normal state.

Beginning at an EF of 100 mV mm^{-1}, keratinocytes show directed migration toward the cathode during threshold determination reaching full directedness at an EF of 200 mV mm^{-1}. This threshold is in accordance with previous reports (Fig. 2B)[28,46]. There is a significant difference in directedness between the control cells (no stimulation) and those subjected to exogenous EFs. The differences in average directedness range from −0.21 for the control to +0.36 ($p < 0.01$) and +0.69 ($p < 0.01$) at 100 and 200 mV mm^{-1}, respectively. There is also a significant difference between the distribution of directed cells between 100 and 200 mV mm^{-1}. At lower EFs, the directedness of movement was not noticeably influenced, as seen in the hairline plots and average directedness for 25 and 50 mV mm^{-1}, respectively. The velocity of keratinocytes is not significantly affected by the presence of an exogenous EF, such that all tested cells exhibit similar migration speeds of around 90 µm h^{-1} on average (Fig. 2C).

After identifying the migration threshold for keratinocytes, they were subjected to alternating stimulation pulses at ±9.5 µA, thus 200 mV mm^{-1} with alternating directionality in device µ1. This experiment is intended to determine if the cellular movement could be switched at will within the microfluidic device using the same pair of electrodes. We could confirm that a switch in EF polarity also reversed the migration, with cells changing direction, migrating alongside the EF lines towards the cathode (Fig. 2D). The reversed polarity of the applied stimulus had an evident impact on the directedness of the cells, with an initial random movement without stimulation followed by orientation towards the current cathode during the stimulation phases. Furthermore, after the first stimulation phase, residual directedness is noticeable during the following 2 h when no stimulation is applied (Fig. 2E). A significant difference exists between the random movement without stimulation and the directed migration with stimulation. During the initial stimulation phase (positive), the keratinocytes showed directed electrotaxis by changing their directedness from +0.05 to +0.49 ($p < 0.01$), with most cells moving towards the right side of the channel (cathode) (Fig. 2F). After polarity reversal, most cells realigned towards the new cathode (left side). They directed their movement throughout the complete stimulation phase, with a new average directedness of -0.39, significantly differing from the non-stimulated cells ($p < 0.01$). During pauses between polarity switching, cells retained significant directedness compared to the non-stimulated control.

The average velocity for non-stimulated and stimulated keratinocytes was significantly lower during polarity switching experiments than monophasic stimulation (Fig. 2G). This decrease could be due to the polarity-switching experiments performed at higher passages, leading to slower motility[47]. Nevertheless, the internal non-stimulated control still justifies the results showing evident directional switching migration of keratinocytes. The results obtained herein are equivalent to previously published investigations on human keratinocytes, thus ensuring that our salt-bridgeless system does not negatively influence the electrotaxis of these cells[28].

Fibroblasts migrate toward the anode. Fibroblasts are larger and less mobile than keratinocytes, as evidenced by the shorter distance traveled by these cells (Fig. 3A). Furthermore, fibroblasts require higher EFs and longer

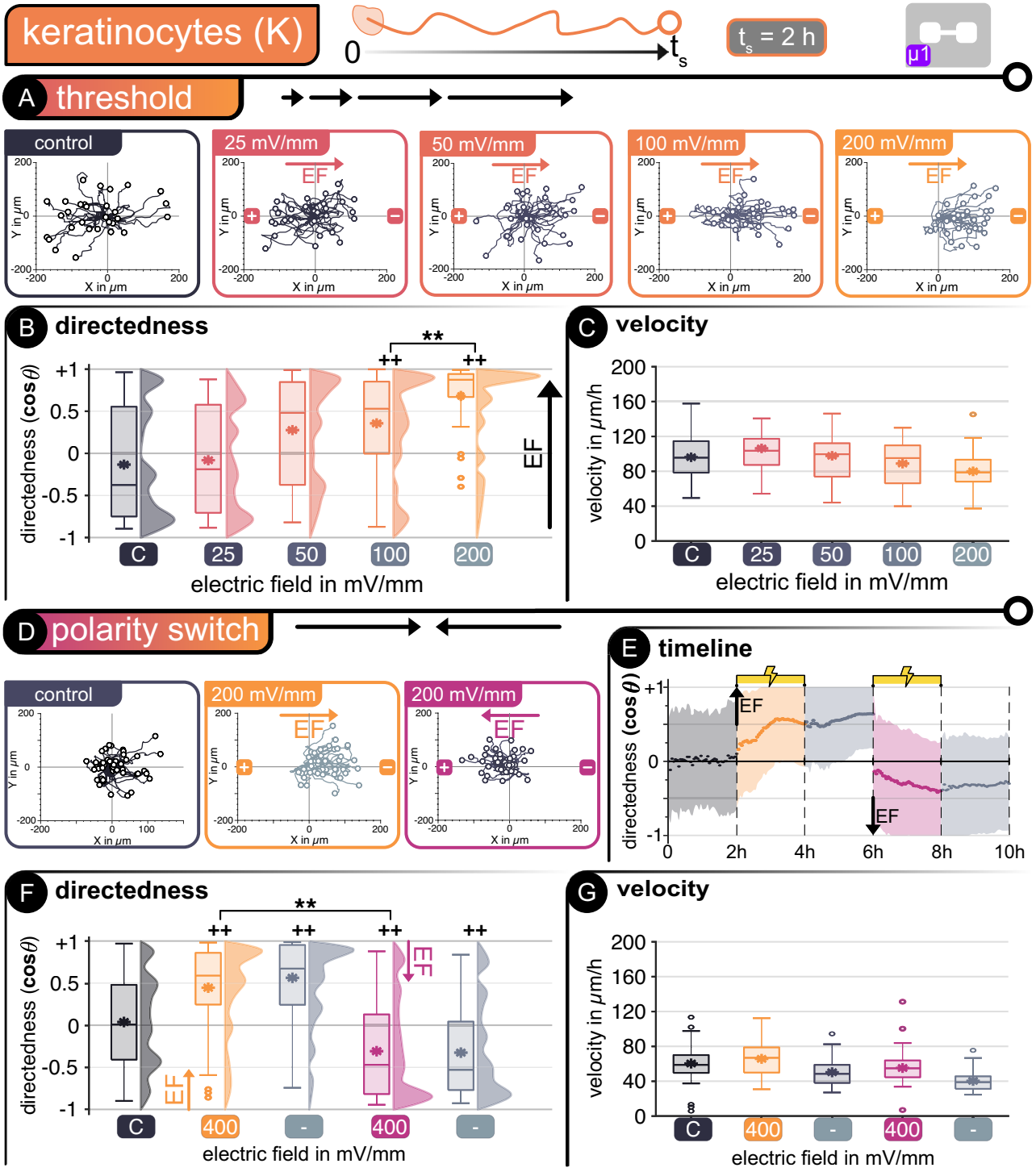

Figure 2. Keratinocytes—*Threshold determination*—(**A**) Cell tracking in microfluidic device *μ1*. Hairline plots represent individual movement over 2 h for non-stimulated and stimulated cells at different electric fields between 25 and 200 mV mm^{-1} (n = 50). Migration statistics (**B**) directedness and (**C**) velocity**.** *Polarity switch*—(**D**) Hairline plots for movement over 2 h for non-stimulated and stimulated cells at alternating electric fields of 200 mV mm^{-1} (n = 50). (**E**) Timeline of polarity switch experiment. Dots represent average every 3 min and shaded area represents standard deviation. Migration statistics (**F**) directedness and (**G**) velocity**.** | For all box plots, the box represents the 1st and 3rd quartiles, middle line shows the median, * denotes the mean value, the whiskers represent the max. and min. values, respectively, and circles represent outliers. + $+p < 0.01$ when compared to the control with no EF. ** $p < 0.01$ when compared amongst stimulated cells of different EF.

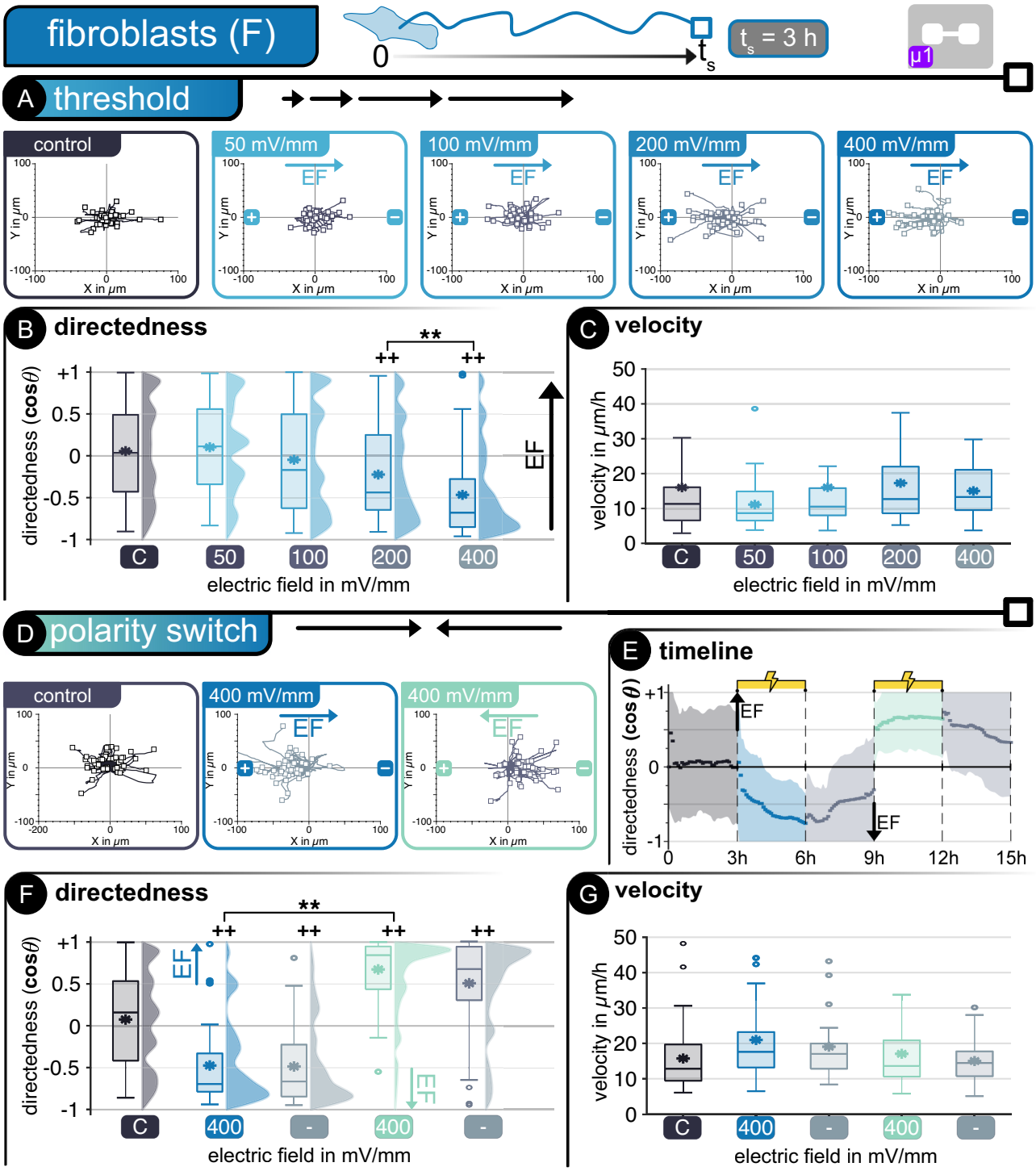

Figure 3. Fibroblasts—*Threshold determination*—(**A**) Cell tracking in microfluidic device *μ1*. Hairline plots represent individual movement over 3 h for non-stimulated and stimulated cells at different electric fields between 50 and 400 mV mm^{-1} (n = 50). Migration statistics (**B**) directedness and (**C**) velocity**.** *Polarity switch*—(**D**) Hairline plots for movement over 3 h for non-stimulated and stimulated cells at alternating electric fields of 400 mV mm^{-1} (n = 50). (**E**) Timeline of polarity switch experiment. Dots represent average every 3 min and shaded area represents standard deviation. Migration statistics (**F**) directedness and (**G**) velocity**.** | For all box plots, the box represents the 1st and 3rd quartiles, middle line shows the median, * denotes the mean value, the whiskers represent the max. and min. values, respectively, and circles represent outliers. + $+p < 0.01$ when compared to the control with no EF. ** $p < 0.01$ when compared amongst stimulated cells of different EF.

stimulation times to show directed electrotaxis. Starting at 200 mV mm^{-1}, directed migration toward the anode is noticeable compared to the non-stimulated cells, with changes in average directedness from + 0.05 to − 0.31 ($p < 0.01$). Increasing the stimulation EF to 400 mV mm^{-1} leads to a more defined distribution of directed cells with a more pronounced directedness of − 0.52, which significantly defers from the non-stimulated (control) and the 200 mV mm^{-1} field ($p < 0.01$). The directed movement influenced by electrical stimulation was not noticeable below 200 mV mm^{-1} with directedness values similar to the non-stimulated cells of + 0.06 and − 0.08 for 50 and 100 mV mm^{-1}, respectively (Fig. 3B). On average, all fibroblasts migrate at approximately 15 µm h^{-1} without any significant difference between non-stimulated and stimulated cells (Fig. 3C).

The influence of polarity reversal during direct current stimulation on fibroblasts was studied at higher currents of ± 15 µA, producing EF values of 400 mV mm^{-1} in alternating directions within device µ1. These cells, analogous to keratinocytes, retain their previously observed electrotactical properties with a clear orientation towards the anode when an external stimulus is applied (Fig. 3D). During the initial phase without stimulation, fibroblasts move randomly, as expected, changing their directedness opposite to the EF lines as soon as stimulation is applied. During the first stimulation phase (positive EF), fibroblasts migrated toward the anode (left). Reversal of the polarity leads to a subsequent reversal in electrotaxis, with most cells reorienting themselves toward the new anode (right). The average directedness of fibroblasts increased with sustained stimulation. This observation is valid for both phases with stimulation. Like keratinocytes, the fibroblasts retain their directedness long after the stimulation is interrupted and slowly transition back to more random movement, similar to their non-stimulated behavior (Fig. 3E). The differences in cellular directedness were significant when compared to non-stimulated cells, with changes in average values from + 0.11 (control) to − 0.65 and + 0.72 for the positive and negative stimulation phases, respectively. Significant changes in directedness compared to the control were also noticeable during the pauses after stimulation phases (Fig. 3F). An average migration velocity of 17 µm h^{-1} was determined for fibroblasts with slightly higher velocity during stimulation (Fig. 3G). These results confirm previous observations on human fibroblasts[18].

Both tests on keratinocytes and fibroblasts demonstrate that a salt-bridgeless system supplying direct current stimulation to the cell media can elicit the expected electrotactical response for both epithelial cells. Furthermore, these results show no noticeable adverse effects on cell mobility or viability. These results provide the baseline for a direct comparison between mono- and co-cultured keratinocytes and fibroblasts.

Co-culture electrotaxis of human skin cells. *Finding a suitable co-culture media.* When establishing a co-culture, it is essential to consider a suitable media that accommodates different cell types. In this study, we focused on the cell media previously employed in mono-cultures to maintain the chemical composition and, thus, the electrical properties of the media the same. The suitability of the media was assessed through imaging (Fig. 4A) and metabolic assessment (Fig. 4B) (c.f., section "Metabolic activity assay"), as cells need to show similar metabolism, morphology, and phenotypes to ensure comparability between mono- and co-culture stimulation. Three media were investigated for mono- and co-cultures of keratinocytes (*K*) and fibroblasts (*F*), mainly serum-free K media (M1), serum-containing F media (M2), and a 1:1 mixture of both (M3) (c.f., Table 1, section "Cell culture media").

We found that *Ks* were more sensitive to media composition than *Fs* and required keratinocyte media (M1) to seed and proliferate effectively. *Ks* in fibroblast media (M2) retained a rounded morphology and did not show the characteristic extension of lamellipodia on the substrate. On the other hand, *Fs* could seed and proliferate in all media but showed less metabolic activity in M1 and M3 compared to control media M2. Co-culture (*KF*) results showed that *Ks* required supplements in M1 to seed and be metabolically active, while mixed media (M3) and M1 were adequate for co-culture metabolic activity. In keratinocyte media (M1), both cell types formed an evenly mixed population, but *Fs* did not have the structured alignment they possess in fibroblast media (M2). In mixed media (M3), *Fs* regained their structured phenotype, and *Ks* formed more cell–cell junctions.

Directional separation of keratinocytes and fibroblasts. After carefully evaluating cell viability and metabolism in an adequate medium for keratinocytes (*Ks*) and fibroblasts (*Fs*) in co-culture, these cells were investigated jointly in a common bioelectronic platform. The co-culture was seeded in a multi-channel microfluidic device (**µ2**) with branching channels through which current at different magnitudes could flow, thus generating a variety of carefully defined EFs to guide cellular migration. Using a drop-cast seeding method of both cell types simultaneously in device µ2 led to the homogeneous distribution of *Ks* and *Fs* within all device channels in all biological replicates, thus allowing reproducible experimentation. The morphology of the cells in the co-culture within the microfluidic channel was similar to the preliminary observations during MTT assays in well plates (Fig. 4A). Fibroblasts were independent, as expected from *F* mono-cultures, while keratinocytes were evenly spread between independent cells and *K* clusters. The difference between mono- and co-cultured *Ks* did not impact their response to the applied EF, as all stimulated cells were reactive to the EF guidance cues throughout the 12 h stimulation. However, it did impact their average directedness, particularly at higher EFs, as *K* clusters needed more room to migrate and had to circumvent *Fs* in some situations.

Ks and *Fs* demonstrated similar behavior in co-culture as in mono-culture, with a characteristic anodic migration for *Ks* and cathodic migration of *Fs*, effectively separating both cell types when stimulation was applied in co-culture (Fig. 5). The presence of both cells within the microfluidic channel had no dramatic influence on their electrotactic properties. In some situations, migration was slightly hindered through cell–cell collisions, but the overall net directedness was unaffected. Though cell density in each channel varied slightly, the influence of the applied EF was clearly distinguishable between *Ks* and *Fs*. Simultaneous cell tracking and overlapping of the hairline plots emphasizes differences amongst these cells in the direction of migration, their migration path, and their velocity (Fig. 5A). The differences in cell size and mobility are further noticeable during imaging, with

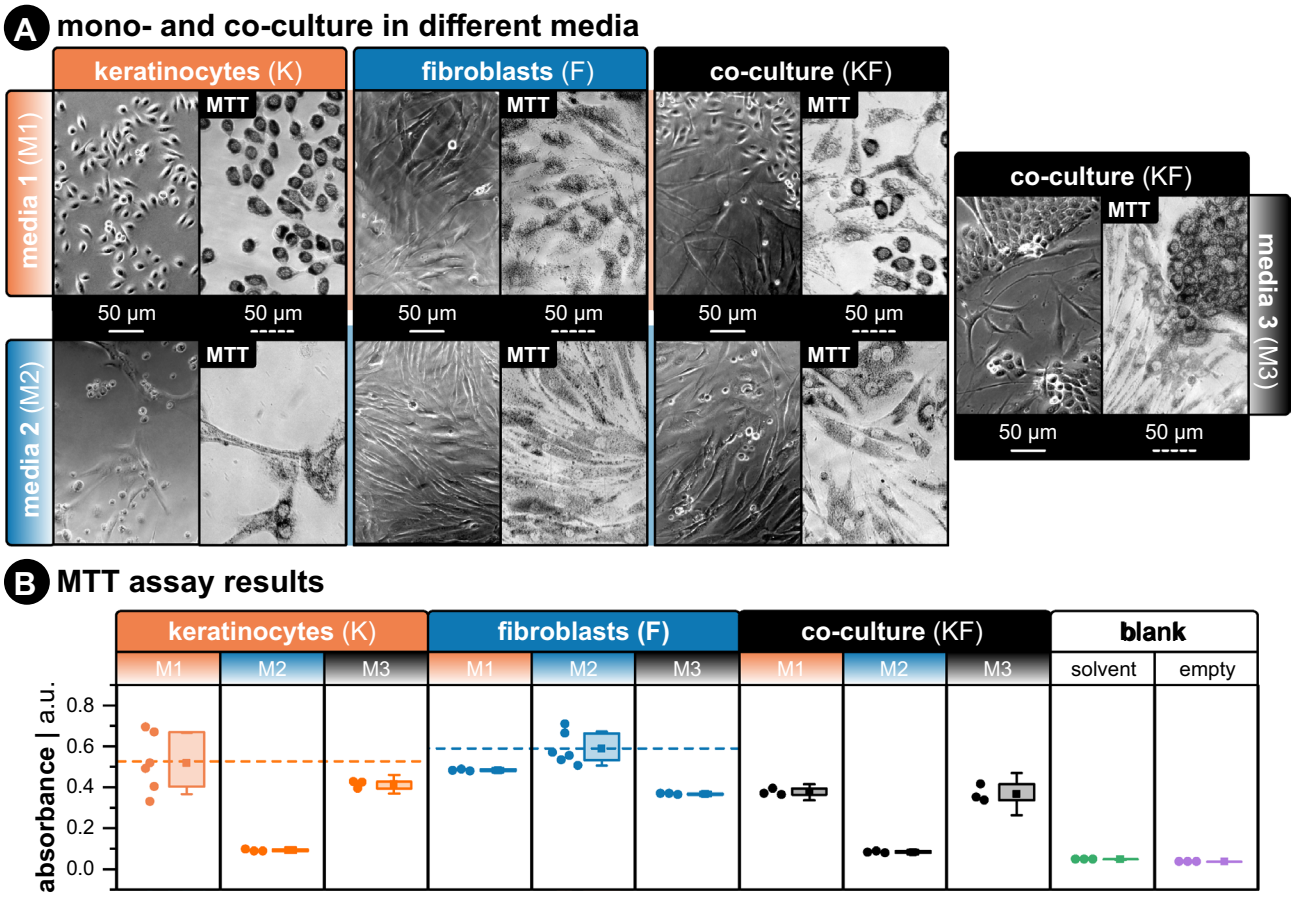

Figure 4. (**A**) Phase-contrast images of keratinocytes, fibroblasts, and a mix of both types in different media. Left panel shows cultured cells 36 h post-seeding. Right panel shows cells with reduced formazan crystals before placing on the plate reader. All cells were seeded into 96-well plates and at the same total number of cells (1×10^5) with the same volume (100 µL). For co-culture wells, the total amount was the same (5×10^4 for K and F). All scale bars are 50 µm. (**B**) Metabolic activity measured by absorbance at 570 nm. More signal correlates to more metabolic activity. The horizontal dashed line for each group corresponds to mean absorbance for the control group (i.e., the media used during mono-culture experiments). The "blank" group shows absorbance results for wells filled with the MTT solvent (i.e., dimethyl sulfoxide—DMSO) or wells that were left empty.

clearly spread-out *Fs* slowly moving through the microchannels and both individual and agglomerated *Ks* swiftly migrating and reorienting themselves to avoid collisions. (Refer to supplementary videos for individual EFs).

Analogous to the mono-cultures (Figs. 2 and 3), a clear impact of the EF magnitude on the directedness of the cells was notable in co-culture, with *Ks* showing significant directedness compared to non-stimulated cells at lower EFs than *Fs*. Both cell types showed similar thresholds in co-culture as in mono-culture, with a significant difference from the non-stimulated control group starting at 120 mV mm^{-1} for *Ks* and 305 mV mm^{-1} for *Fs* (Fig. 5B). Co-cultures were stimulated for longer periods than mono-cultures leading to more pronounced directedness at EFs below the previously established thresholds, similar to previous observations in the literature about mono-cultures[28,48]. Increasing the EF magnitude led to more defined directedness in *Fs* analogous to observations in mono-cultures. However, this effect was not observable for *Ks*, with cells showing a lower degree of directedness at 205 mV mm^{-1} compared to the mono-culture and losing directed migration at the highest EF applied. Stimulated *Fs* and *Ks* showed no significant change in their migration velocity under the influence of an externally applied EF compared to non-stimulated control cells, analogous to the individual investigation of each cell type. A difference in velocity between the mono-cultured and the co-cultured cells is notable, particularly for *Fs*. These cells increased their migration velocity by approximately 50% to 23 µm h^{-1} when in co-culture, whereas the *Ks* retained similar speeds as the mono-cultured ones. (Fig. 5C).

A further distinction between the co-cultured *Fs* and *Ks* and their mono-cultured counterparts is noticeable in the changes of directedness over time, particularly for higher EFs, where both cells show significant differences from non-stimulated cells. Figure 5D shows a comparison between *Fs* and *Ks* directedness without stimulation (control) and under an EF of 305 mV mm^{-1}. Non-stimulated cells show random movement for 12 h, while stimulated cells slowly direct their movement alongside (*Ks*) and opposite (*Fs*) to the EF lines. This alignment is slower for co-cultured cells than for mono-cultured ones reaching a maximum directedness after 6 h of stimulation. Nonetheless, a defined cellular separation is notable, as expected from the individual behavior of each cell type. These results respond both questions of this work (Fig. 1), as *Fs* and *Ks* could be successfully cultured together,

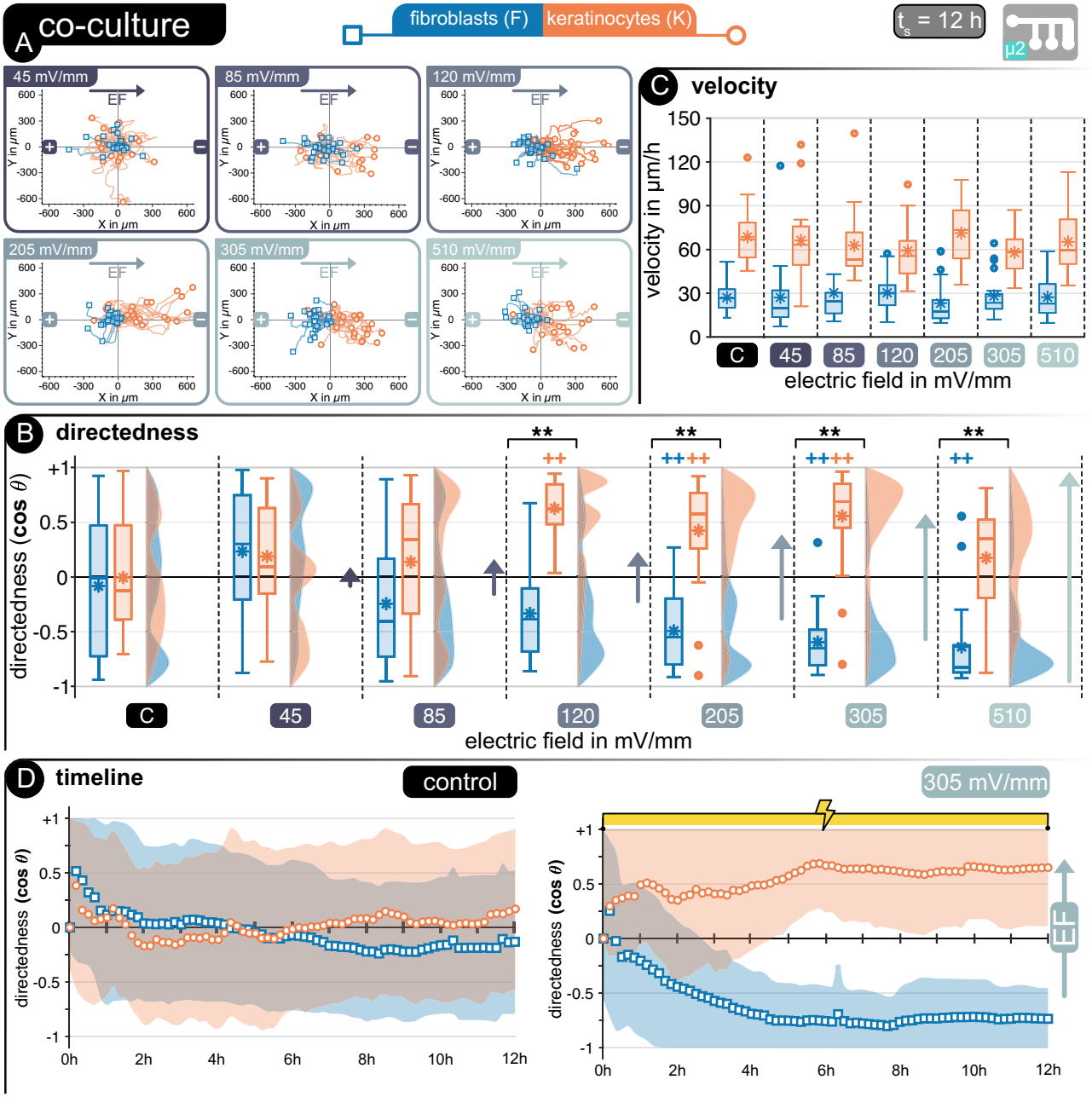

Figure 5. Co-Culture—(**A**) Cell tracking in microfluidic device *μ2* for keratinocytes (orange) and fibroblasts (blue). Hairline plots represent cell movement over 12 h of stimulated cells at different electric fields between 45 and 520 mV mm^{-1} (n = 25/cell type). Migration statistics (**B**) directedness and (**C**) velocity for keratinocytes (orange) and fibroblasts (blue). (**D**) | For all box plots, the box represents the 1st and 3rd quartiles, middle line shows the median, * denotes the mean value, the whiskers represent the max. and min. values, respectively, and circles represent outliers. + $+p < 0.01$ when compared to the control with no EF. ** $p < 0.01$ when compared amongst cell types at same EF strength.

retaining their electrotactic properties and aligning themselves to externally applied EFs. Furthermore, both cell types showed an analogous electrotactic response in co-culture and mono-culture.

Discussion

Human epidermal keratinocytes (*Ks*) and dermal fibroblasts (*Fs*) reside in different layers of the human skin and are typically not merged in planar co-cultures. Nevertheless, it has been shown that these cell types concurrently influence each other during the healing process of wounds, and the underlying mechanisms governing this interaction still need to be elucidated[31,49,50]. The electrotactic behavior of human *Fs* and *Ks*, as well as the suspected underlying mechanisms that lead to the directed migration alongside an EF, such as calcium channel activation and PI3K signaling, have previously been proposed and investigated[18,51]. However, these experiments

have usually been done on one cell type at a time, thus relinquishing the active interactions between different cell types in their usual biological environments. Limitations here have been mainly due to difficulties of concurrent growth of different cell types within microfluidic devices and the employed stimulation setup and electrodes. This study carefully investigated the electrotactic behavior of both cell types. First, individually, serving as a jumping-off point to determine the adequacy of a salt-bridgeless stimulation setup to study the electrotactic response of human skin cells. Second, their electrotactic behavior was reproduced and evaluated in co-culture experiments.

Co-cultured fibroblasts and keratinocytes were successfully stimulated within device **µ2** and reacted to direct current stimulation, with clear distinction in the directedness of movement for both cell types. Furthermore, both cells began electrotaxis at the expected EF strengths, as determined during the initial threshold experiments on mono-cultures. One of the key points we want to highlight in this work is that neither the seeding method, the stimulation protocol, nor the employed salt-bridgeless electrodes negatively impacted the cells but rather confirmed and expanded on electrotaxis dose–response findings of human keratinocytes and fibroblasts. Therefore, a clear cellular partition was achievable under the chosen biological and electrical conditions (Fig. 5). Keratinocytes migrated distinguishably towards the cathode, regardless of the new morphological phenotype (clusters) obtained in the new media, while fibroblasts concurrently migrated in the opposite direction towards the anode. The observed behavior is not representative of how wound healing typically happens, with an initial underlying fibroblast migration for restructuring, followed by the keratinocyte migration towards the wound center for re-epithelization. However, these newly validated platforms can be further leveraged to investigate how different biological factors are orchestrated (e.g., plasma, serum transition) during typical wound healing mechanisms.

Experimentation of these cell lines in co-culture under the same stimulation paradigms has not been demonstrated[52]. As these cells require different conditions to be viable in culture, identifying a suitable cell media for coexistence in vitro was fundamental. Here three main factors were considered: (i) the new media needed similar calcium concentration as the media for individual cells; (ii) it should allow for clearly distinct morphological phenotypes between cell types (if no fluorescent tagging or cell-specific surface reporters are used), thus allowing differentiation amongst cell types during tracking; (iii) and it should not significantly diminish the metabolic activity of the cells. After several combinations, a one-to-one ratio between fibroblast and keratinocyte media was chosen. Both cell types were metabolically active with slightly lower activity in the new media (M3) in comparison to mono-cultured cells in their respective media (M1, M2), the media had comparable calcium concentrations required for electrotaxis, and the cells could be easily distinguished from each other. Fibroblasts showed similar morphology as in their individual media, while keratinocytes formed two phenotypes of individual keratinocytes and keratinocyte clusters (KCs) (Fig. 4).

This higher degree of KCs directly correlates to the media's calcium concentration[53]. In mammalian skin, there is a calcium gradient from the apical layer (highest calcium concentration with terminally differentiated keratinocytes and strong cell–cell adhesion) to the basal layer (lowest calcium concentration with proliferating keratinocytes and weak cell–cell adhesion)[54,55]. Also, fibroblasts require extracellular calcium concentrations above 1.4 mM to proliferate[54]. In culture, the same modulation of cell–cell adhesions can be adjusted with calcium concentration[51,56]. Note that the calcium chloride ($CaCl_2$) in keratinocyte media (M1), which is a basal media, is 0.06 mM, and in fibroblast media (M2), it is 1.80 mM. Therefore, in the mixed media (M3), it was set to 0.93 mM. The compromise of extracellular calcium concentration on keratinocyte and fibroblast proliferation explains why for the same number of cells, the metabolic activity was lower in the co-culture with M3 compared to *Ks* in M1 and *Fs* in M2. The combination of the metabolic activity results and the formation of distinct subpopulations of *Fs* and *Ks* with strong cell–cell adhesions, which favors cell tracking, led us to choose the mixed media (M3) for all co-culture experiments.

These quantifiable and observable metabolic and phenotypical differences are a response to the media composition and were expected to play a significant role in the cells' migration and reaction to an externally applied EF in addition to the intercellular interactions. However, once stimulation was applied, the cells' net response to the stimulation in co-culture was on par with the established mono-culture reaction. Similar electrotactic thresholds of 100–120 mV mm^{-1} for *Ks* and 200–205 mV mm^{-1} for *Fs* were determined in mono- and co-culture, respectively, thus evidencing that the chosen media combination was suitable for the direct comparison of the stimulation's effect on cellular electrotaxis. This provides new insights into how an externally applied EF can overpower metabolic and phenotypical differences in cells even when cultured together resulting in controlled directed migration. The platforms presented here can be implemented in future research on the keratinocyte-fibroblast interaction through a combination of DCs and variations of media composition to simulate the naturally occurring homeostatic changes during wound healing and validate how exogenous EFs regulate and possibly overpower cellular migration and intercellular interactions[29,57].

The results obtained during the initial experiments with device *µ1* are on par with previously postulated electrotactic parameters for both *Ks* and *Fs*[28,30,48,58]. These results further emphasize that a salt-bridgeless system does not negatively influence cellular behavior, facilitating the experimental setup. The fundamental characterization of keratinocytes (Fig. 2) and fibroblasts (Fig. 3) provides valuable insights for the future development of bioelectric wound dressings aimed at wound healing acceleration through cell migration redirection. When stimulating *Ks* and *Fs* separately, the experiment can continually be optimized to the respective cell type. We argue that co-culture experiments have an essential role to fill, as these results demonstrate that a relevant response can be triggered in both types of cells, even when trade-offs have to be made between what the optimal environment for *Ks* and *Fs* is and how these compromises impact cell migration and intercellular interactions, respectively. It is a small but crucial step closer to real-world application. It should be noted that the differences in migration direction, cathodic for keratinocytes and anodic for fibroblasts, are known behaviors for which a clear explanation is still missing. Several hypotheses have been postulated trying to explain the directional choice of these cells involving calcium signaling pathways[54,55,59], PI3 kinase (PI3K)[18,60], transforming growth factor-β3 (TFG-β3)[61], Golgi polarization[62], or integrin expression[63], nonetheless, a clear consensus remains elusive. A natural next step

for future work is exploring to which extent the electrotactic response reported in single cell cultures, and here further validated in co-cultures, is preserved in three-dimensional constructs more closely mimicking actual skin. The salt-bridgeless electrode concept demonstrated here is easily transferrable to such complex cultures, as the electrodes and the stimulation supplied remain biocompatible and do not need buffer layers to protect the treated cells. Furthermore, the electrodes are customizable in size and geometry through laser structuring or photolithographic processes.

Skin wounds might seem inconsequential in everyday life for most people, as the skin heals itself over days to weeks without much conscious maintenance. For the skin itself, however, this process requires a plethora of different cell types, signaling molecules, and communication pathways as it undergoes the four stages of hemostasis, inflammation, proliferation, and remodeling[64]. A better understanding of the underlying cellular mechanisms involved in electrotaxis, as well as technical solutions that allow translation from in vitro testing to in vivo applications, are required to develop successful clinically validated wound therapy based on direct current stimulation[45,65–73]. This study discusses two devices and electrodes designed to facilitate electrotaxis experimentation. Both devices have advantages and drawbacks and can be leveraged based on the desired purpose. The PDMS and PMMA devices used in the study have proven reliable for electrotaxis research. They provide a suitable environment for cell seeding and proliferation and enable direct current stimulation of different cell populations without the need for salt bridges. The second device and its drop-cast seeding approach make co-culture seeding and experimentation straightforward, allowing for future exploration of more biologically relevant constructs.

We believe this work is just the beginning of studying co-cultured keratinocytes/fibroblasts electrotaxis, as the technology devised here can significantly facilitate further experimentation in co-culturing these cells under different biological conditions in order to identify which limits and cues govern cellular migration in real wounds. Furthermore, the results presented here utilizing salt-bridgeless electrodes bring us one step closer to leveraging electrical stimulation for cellular steering in clinical settings. Now the sandbox is filled for other researchers to play and explore the bioelectric communication and mechanisms between these two cell types.

Conclusion

In this work, we demonstrate that human fibroblasts and keratinocytes can be electrotactically guided in a salt-bridgeless system concurrently, retaining their expected electrotaxis, thus leading to the directional separation of both cell types. We leveraged two different microfluidic systems compatible with different salt-bridgeless electrodes that facilitate in vitro experimentation with cell cultures, particularly on the effects of DC stimulation on cellular electrotaxis. All cells tested in this study showed the expected electrotactic behavior under the influence of an externally applied EF with directedness toward the cathode for keratinocytes and the anode for fibroblasts, both in mono- or co-culture. Furthermore, both cells could be guided at different EF strengths and polarities. A suitable media combination was determined for the viability of the cells in co-culture and was found to lead to an evident change in keratinocyte agglomeration and metabolic rate of both cell types. However, the applied EF was the dominant force as keratinocytes and fibroblasts displayed similar electrotactic behavior in co-culture and mono-culture. This study demonstrated for the first time the concurrent seeding, growth, and electrotactic stimulation of co-cultured human keratinocytes and fibroblasts in a microfluidic device. We propose a new approach for cell seeding and direct current stimulation for the concurrent investigation of both cell types involved in several stages of wound healing, thus opening the door to faster and straightforward in vitro characterization and investigation of different environmental, chemical, and metabolic cues alongside EF stimulation, as well as potential future clinical applications of direct current stimulation therapy.

Methods

Compact microfluidic platforms with salt-bridgeless electrodes. Microfluidic devices allow precise control of the electric field (EF) distribution through accurate fabrication, known media composition, and precise current control, thus ensuring that all cells studied are subjected to the same stimulus. This is possible as the EF inside a rectangular channel, as the ones employed in this study, is directly dependent on the channel's cross-section (width—w, height—h), the conductivity of the fluid in the channel (σ), and the applied current I following Ohm's law:

$$EF = \frac{I}{w \times h \times \sigma} \tag{1}$$

Here we utilize two approaches to microchannels in the form of a single-channel (**µ1**) and a multi-channel (**µ2**) device (Fig. 6A). The determination of the applied EF is straightforward in device µ1, as the cross-section is well-defined and current flows through the channel, the EF distributes homogeneously across the experimental area. The small cross-section achievable through soft-lithography on PDMS leads to high EFs utilizing a relatively small current. However, the current must be sequentially changed to achieve different EFs with this device. On the other hand, the multi-channel microfluidic device µ2 provides six different EFs utilizing one set current. It serves as a current divider and subsequently an EF divider, resulting in 6 different regions with EF ratios of 13 : 8 : 5 : 3 : 2 : 1, as validated through FEA analysis (Fig. 6B).

Fabrication of microfluidic devices. *Device 1: more complex but higher geometrical precision.* These devices were fabricated according to protocols according to Leal et al., as a guide, please see Fig. 6C[42]. The microfluidic channels ($3 \times 0.3 \times 0.1$ mm^3–l × w × h) were fabricated through soft lithography of two-component polydimethylsiloxane (PDMS) Sylgard 184 (Dow Corning, MI, USA) onto SU-8 structures. The PDMS was heat cured at 65 °C, and subsequently, the independent structures and the media reservoirs ($10 \times 10 \times 2$ mm^3) were cut. Finally, the devices were plasma treated for 2 min at 300 W, air flow of 10 sccm, and a pressure of 0.8 mbar

before being irreversibly bonded to a glass slide. The addition of OH groups on the PDMS walls increases the hydrophilicity of the channel, thus facilitating flow-through cell seeding.

Device 2: more flexibility and larger feature size. As a guide, please see Fig. 6C. Besides the sterile polystyrene dish, all microfluidic device components are fabricated with a 30 W carbon dioxide (CO_2) laser (Universal Laser Systems, VLS 2.30). For the acrylic-based double-sided pressure-sensitive adhesive (Adhesives Research, 90445Q), a kiss-cut was made with 7.5 W at 70 mm s^{-1}, and a through-all cut was made with 24 W at 70 mm s^{-1}. The bottom-side liner (i.e., without the kiss-cut) was first peeled off to expose the bottom-side adhesive, then was pressure-bonded by hand to a new Petri dish. Importantly, batches of dish/adhesive were placed in a vacuum desiccator overnight to remove any air bubbles during bonding. These are stored on the shelf until further use. The acrylic (Modulor, Germany) two-part lid consists of a thin 0.5 mm base that only has fluidic vias and a thicker 8.0 mm reservoir-defining layer (Fig. 1c, pink part). These two parts were solvent-bonded together using dichloromethane (Modulor, Germany). Note that this lid is not bonded to the microfluidic adhesive until the cells are seeded (see section "Cell lines").

Seeding of microfluidic devices. *Device µ1: flow-through seeding.* The protocol used here follows Leal et al[42]. The PDMS devices were immersed in 70% ethanol for 30 min for sterilization and then placed in sterile PBS (Carl Roth GmbH + Co. KG, Karlsruhe, Germany) for 1 h before cell seeding. Before the seeding procedure, the devices were dried, and any remaining PBS inside the channel was carefully aspirated. Subsequently, a 10 µL droplet with approximately 10^3 cells μL^{-1} was pipetted at the entrance of the microchannel, and the media and cells were driven within the channel through capillary forces. The devices were subsequently placed in an incubator (37 °C, 5% CO_2) for 3 h to permit cell attachment on the glass. After cell adherence, the media reservoirs were filled with 200 µL of the corresponding media for each cell line, M1 for keratinocytes and M2 for fibroblasts (see section "Finite Element Analysis (FEA)").

Device µ2: drop-cast seeding. The protocol used here follows Shaner et al[35]. Petri dish devices were first washed with 70% ethanol and nitrogen dried. Then the devices were air plasma-treated (Femto, Diener Electronics) on the same day as seeding to improve cell adhesion. The settings were 30 W, 3 min, and 10 sccm air. The dishes were soaked in 70% practical grade (p.a.) ethanol under the cell culture hood (Safe 2020, Thermo Scientific) for 15 min before washing with sterile water, then allowed to dry in the hood. Lastly, the devices were subjected to the hood's integrated UV lamps for 1 h. Sub-cultured keratinocytes or fibroblasts were harvested into the desired concentration (5×10^5 cells mL^{-1}). A volume of 100 µL of this suspension was seeded (5×10^4 total cells) directly onto the open microchannels and incubated for 3 h to allow for cell attachment. Afterward, 10 mL of fresh media is added and placed back into the incubator for one to three days. After the desired confluency was achieved, the media was aspirated until only a small amount of media resided in the microchannels leaving the liner as dry as possible. The liner was then peeled, and the two-part acrylic lid was aligned and fixed using alignment marks etched into the adhesive. Media was immediately replenished by initially flowing 100 µL directly into the microchannels to displace trapped air, and then the wells were filled with more fresh media. The electrodes were assembled and placed into the reservoir, and the corresponding wires were routed through the lid, which was applied to prevent evaporation.

Finite element analysis (FEA). The microfluidic devices were designed and exported (IGS file extension) in Solidworks (version 2021). COMSOL Multiphysics® software (version 5.3) was used to simulate EF distribution using the Electric Currents module. For EF distribution, electrodes sat on top of the reservoirs and were modeled to have the electrical conductivity of PEDOT:PSS hydrogels ($\sigma = 2000$ S m^{-1})[74]. The media was modeled with an electrical conductivity (σ) of 1.5 S m^{-1}, which was measured for all three media options using a portable conductivity meter (DiST6 EC/TDS, Hanna Instruments, Germany). The relative permittivity of the media was 80, which is typical for saline water. The cathode was set to 0 V. The input current density (placed at the face of the anode) was swept to identify which input current is needed to achieve the desired EF strengths.

Fabrication of electrodes. *Metal electrodes coated with conducting polymer.* The protocol used here follows Leal et al[42]. In short, thin-film electrodes consisting of 300 nm platinum tracks with 700 nm of Sputtered Iridium Oxide Film (SIROF) active sites sandwiched between 10 µm of polyimide insulating film were fabricated in a Class 3 clean room at the University of Freiburg. These devices had an active electrode area of 20 cm^2 onto which the conducting polymer poly(3,4-ethylenedioxythiophene) polystyrene sulfonate (PEDOT/PSS) was electrochemically polymerized. This was done from an aqueous solution containing sodium polystyrene sulfonate (NaPSS, 5 mg mL^{-1}) and 3,4-ethylenedioxythiophene monomers (EDOT, 0.01 M) (Sigma Aldrich, MO, USA). The electropolymerization was done with a high-precision potentiostat/galvanostat (PGSTAT204, Metrohm Autolab B.V., Filderstadt, Germany). A three-electrode setup was employed in which the probe to be coated served as the working electrode (WE), a silver/silver-chloride (Ag/AgCl, BASI, USA) electrode as the reference (RE), and a stainless-steel sheet (≈2 cm^2) as the counter electrode CE. The WE was driven at 0.9 V while the charge passing through the electrode was measured and utilized as a proxy to determine the polymer thickness. All electrodes were coated until 60 µC was reached, equivalent to a charge density of 300 mC cm^{-2}.

Non-metal electrodes coated with conducting hydrogel. The protocol used here follows Shaner et al[43]. In short, the base electrode material was fabricated on the surface of thin sheets (75 µm) of polyimide (Kapton HN, Dupont, USA) and was carbonized using a mid-IR (wavelength of 10.6 µm) CO_2 laser (VLS 2.30, Universal

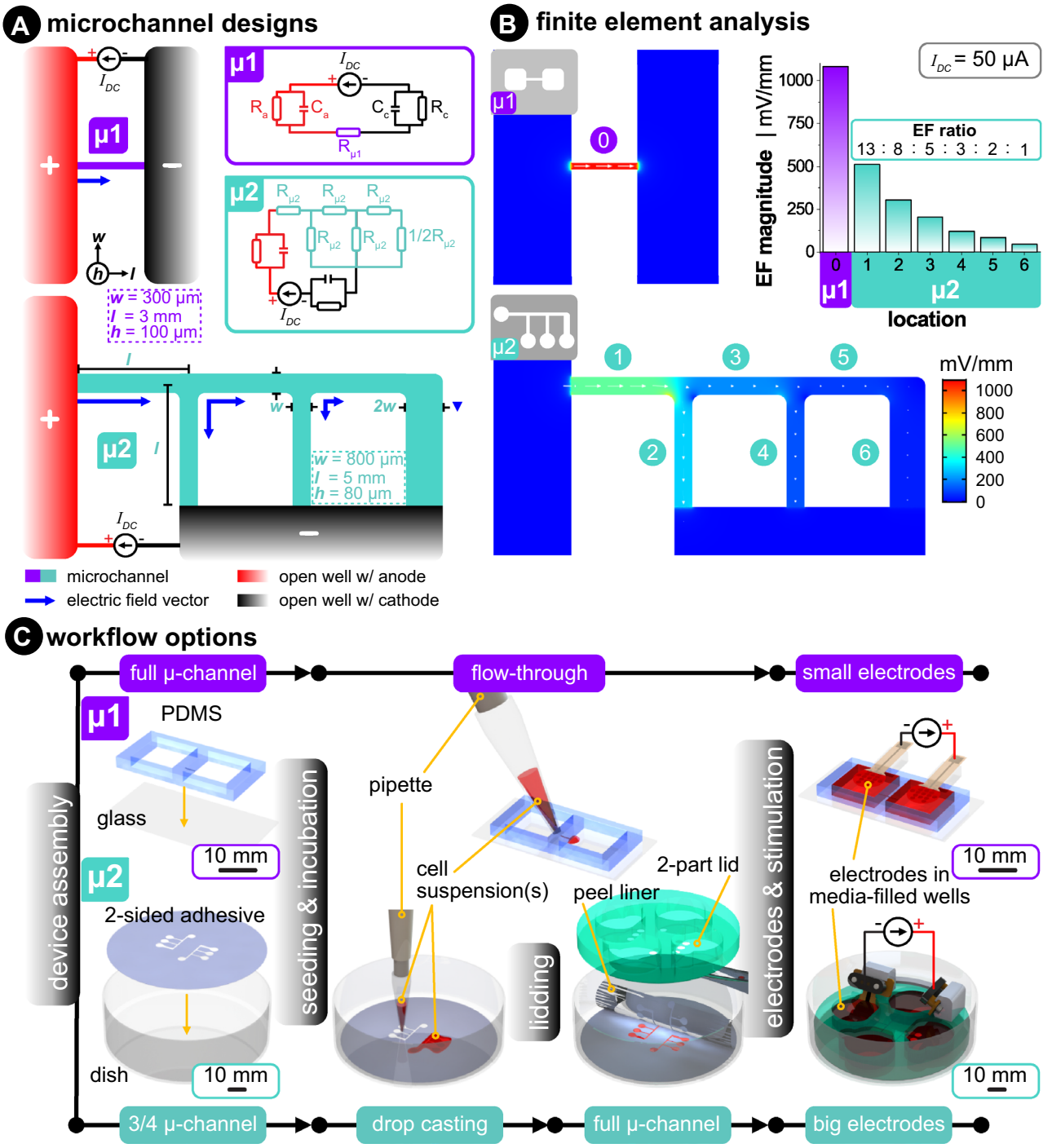

Figure 6. (**A**) Device **μ1** (violet) shows a top view of a simple rectangular microchannel that connects two open wells, each filled with excess media (mL in the wells and μL in the microchannel). Device **μ2** (turquoise) shows a branching microchannel network that forms a current divider. Insets of the electrical equivalent circuit relate the microchannels to resistors and include the electrode–electrolyte interface of both the anode and cathode. (R = resistance, C = capacitance, and I_{DC} = DC source). (**B**) Three-dimensional finite element analysis of both microchannel designs. The same input current (I_{DC} = 50 μA) was used for both cases. The color scale and white arrows signifies the EF magnitude and direction, respectively. (**C**) Two different workflow options used in this paper allow for protocol flexibility. μ1 is made via soft lithography of molded polydimethylsiloxane (PDMS) that is irreversibly bonded to glass via air plasma exposure. μ2 is made by bonding the bottom side of a laser-structured double-sided adhesive to a Petri dish. Cell suspension(s) are flow-through seeded in μ1 and drop-casted in μ2. After cell seeding and growth in μ2, the adhesive's top protective liner is removed, and an acrylic lid is added to complete the microchannels. Once the desired cell confluency is obtained, electrodes are added and stimulated in an incubated microscope.

Laser Systems, USA). This process yields a material called laser-induced graphene (LIG). The LIG was coated with a pure PEDOT:PSS hydrogel to improve electrochemical properties. Specifically, the PEDOT:PSS dispersion (1.3% in water) was spiked with 15% dimethyl sulfoxide (DMSO) and cast onto the amine-functionalized and polyurethane-coated LIG, which improves adhesion between the LIG and hydrogel. PEDOT:PSS hydrogel-coated LIG electrodes were stored in 1 × phosphate-buffered saline (PBS) until further use.

Cell lines. Human epidermal keratinocytes immortalized with HPV-16 E6/E7 were courtesy of Prof. Dr. rer. nat. Thorsten Steinberg (Department of Dental, Oral and Jaw Medicine; University Clinic Freiburg). Human tissue was obtained from healthy patients with their informed consent according to the Helsinki Declaration, and the protocol was approved by the ethics committee of the University of Freiburg, Ethics Approval Nr. 552/18. Primary keratinocytes from epidermal tissue were established as described in Tomakidi et al[75]. Primary human epidermal keratinocytes were immortalized according to the protocol published by Halbert et al[76]. using amphotropic recombinant retroviruses. In this approach, DNA fragments containing the contiguous region encoding E6 and E7 from HPV16 were cloned in the retrovirus vector pLXSN. Following infection, one clone (clone #8) was chosen for long-term propagation in serum-free keratinocyte growth medium (KGM, Promocell, Heidelberg, Germany) containing G418 (50 g/ml) for selection, until cells had reached passage 6. One year after infection, when the cells had undergone approximately 30 passages, they were defined as immortalized and stored in liquid nitrogen at the department of Oral Biotechnology, Medical Center, University Clinic Freiburg. The use of these cells in this study has been approved by the ethics committee at the University of Freiburg, according to Ethics Approval Nr. 411/08.

Human primary fibroblasts P9, PN 109, were courtesy of Prof. Dr. rer. nat. Thorsten Steinberg (Department of Dental, Oral and Jaw Medicine; University Clinic Freiburg). Human tissue was obtained from a 43 year old, male patient from the skin of the abdominal wall with his informed consent according to the Helsinki Declaration, and the protocol was approved by the ethics committee of the University of Freiburg, Ethics Approval Nr. 552/18. These cells have not been genetically modified and its use in this study has been approved by the ethics committee at the University of Freiburg, according to Ethics Approval Nr. 411/08.

Cell culture media. Keratinocytes were cultured in serum-free keratinocytes growth medium (KGM2, PromoCell, #C-39016) supplemented with bovine pituitary extract, epidermal growth factor, insulin, hydrocortisone, epinephrine, transferrin, and $CaCl_2$ provided by the same manufacturer (SupplementMix, PromoCell, #C-20011), as well as neomycin (Sigma-Aldrich, #N1142) at final concentration 20 µg mL^{-1} and kanamycin (Sigma-Aldrich, #K0254) at final concentration 100 µg mL^{-1}. This keratinocyte media is referred to as M1 in Fig. 4.

Fibroblasts were cultured in low-glucose Dulbecco's modified Eagle's media (DMEM, Sigma-Aldrich, #C-22320022) with 10% fetal bovine serum (FBS, Sigma-Aldrich, # F0804). This media was supplemented with the same concentration of neomycin and kanamycin as M1. This fibroblast media is referred to as M2 in Fig. 4. The final media used was a 1:1 mixture of M1 and M2. This co-culture media is referred to as M3 in Fig. 4. Cell culture was incubated at 37 °C and 5% CO_2 at 95% humidity and routinely passaged when 80 to 90% confluency was reached. Growth medium was exchanged three times per week. All experiments in this work included keratinocytes between passages 14–40 (low passages 14–33 were used for threshold characterization, and high passages 34–40 were used for other experiments) and fibroblasts between passages 9–11.

Code Name (Fig. 4)	**M1**	**M2**	**M3**
Abbreviation	**KGM2**	**DMEM**	**50% KGM2 + 50% DMEM**
Additives	- Bovine pituitary extract		(50%)
	- Epidermal growth factor		- Bovine pituitary extract
	- Insulin		- Epidermal growth factor
	- Hydrocortisone	+ 10% fetal bovine serum	- Insulin
	- Epinephrine	+ Neomycin (20 µg ml^{-1})	- Hydrocortisone
	- Transferrin	+ Kanamycin (100 µg ml^{-1})	- Epinephrine
	- $CaCl_2$		- Transferrin
	- Neomycin (20 µg ml^{-1})		- $CaCl_2$
	- Kanamycin (100 µg ml^{-1})		(50%)
			+ 10% fetal bovine serum
			(100%)
			± Neomycin (20 µg ml^{-1})
			± Kanamycin (100 µg ml^{-1})
Cell Type	Keratinocytes	Fibroblasts	Keratinocytes + Fibroblasts

Table 1. Composition of media used in mono- and co-culture experiments and MTT assay.

Threshold determination		
	Keratinocytes (K)	Fibroblasts (F)
t_s [min]	120	180
EF [mV mm^{-1}]	25–50–100–200	50–100–200–400
Polarity reversal		
	Keratinocytes (K)	Fibroblasts (F)
t_s [min]	120	180
EF [mV mm^{-1}]	200	400

Table 2. Parameters for threshold determination and polarity reversal in the single-channel microfluidic device µ1.

Metabolic activity assay. Co-culture media options were evaluated via a cellular metabolic activity assay (i.e., MTT assay). First, cells were seeded (10^6 cells mL^{-1} in 100 µL) in a 96-well plate. The plate was incubated for two days; then, the MTT assay was performed. The MTT reagent (mono-tetrazolium salt) was dissolved in sterile 1 × PBS (5 mg mL^{-1}. This solution was filtered through a 0.2 µm filter via a syringe into a sterile container. 10 µL of the MTT solution was added to the 100 µL-filled wells, then incubated for 3 h at 37 °C. Since the media contains phenol red, the media was carefully aspirated, and the salt crystals were dissolved with 100 µL of sterile 100% DMSO. The plate was placed on a shaker for 5 min at 600 RPM. The absorbance was measured at 570 nm using a plate reader (Enspire, Perkin Elmer GmbH, Germany).

Live-cell imaging and direct current stimulation. Seeded devices were placed in an incubated inverted microscope (Zeiss Axio Observer with Definite Focus 2) and maintained at 37 °C and 5% CO_2. Phase-contrast images were acquired every 3 min for the mono-culture and 10 min for the co-culture devices using a 10X or 5X objective, respectively.

Constant monophasic DC stimulation (1 to 15 µA for the mono-culture device and 50 µA for the co-culture device) was carried out using a potentiostat/galvanostat (PGSTAT204, Metrohm, Autolab). The current densities used for mono-culture experiments were 0.05 to 0.75 A m^{-2}; for the co-culture experiments, it was 0.28 A m^{-2}.

Threshold determination. For threshold determination, device 1 (µ1) was employed. After cell seeding, a train of stimulation phases of increasing currents was applied in monophasic direction with 30 min pause between the increments. The stimulation time t_s was adjusted for each cell type individually. The parameters used in this study are listed for each cell type in Table 2.

Polarity reversal. For polarity reversal studies, device 1 (µ1) was employed. After cell seeding, the cells were stimulated in alternating directions, starting with a positive current and then a negative one, with 30 min pause between the switches. The stimulation time t_s was adjusted for each cell type individually. The parameters used in this study are listed for each cell type in Table 2.

Cellular separation. For cellular separation studies, device 2 (µ2) was utilized. Cells were stimulated for $t_s = 12$ h at a constant current of $I = 50$ µA. Different electric fields were achieved within the microfluidic device due to its design with branching electrical resistance.

Cell tracking. Time-lapse images were pre-processed with FIJI (ImageJ) to improve contrast, sharpen, and align the frames to the direction of the applied EF. Subsequently, cell tracking was done with the CellTracker toolbox for MATLAB (MathWorks, MA, USA) developed by Piccinini et al[77]. For each EF tested, as well as for the control experiments, 50 cells were chosen. For the co-culture experiments, 25 keratinocytes and 25 fibroblasts were tracked. The cells were chosen randomly across biological replicates and tracked manually, leaving out any cell that underwent mitosis or left the field of view. The tracked cells were analyzed and plotted in MATLAB to determine their electrotactic parameters:

- **Cell movement:** cell position in x and y were determined at each time point by the distance and angle from the origin and were plotted with their origin being the x–y position at $t = 0$.
- **Directedness (cosθ):** the angle **θ** was defined as the angle between the EF (x-axis) and the migration vector $\overrightarrow{AB}$ with A being the cell position at $t = 0$ and B the position at each subsequent time point. We defined the position of the cathode **(−)** to the right and the anode **(+)** to the left of the image. A directedness of 0 equals movement perpendicular to the EF, whereas a value of + **1** represents cathodic and **-1** anodic migration, respectively.
- **Average velocity:** determined by the distance traveled by each cell between frames, divided by the time elapsed

Statistical analysis. For each experiment, three biological replicates were done under the same conditions. The tracked cells for each replicate were chosen randomly from different locations within the microfluidic devices, and then the data from each position and replicate were pooled to have at least 16 ± 1 cells per replicate to reach

50 total. A Student's t-test with a 99% confidence interval was used to assess the significance of the differences between the directedness and velocity of the non-stimulated and stimulated cells.

Data availability

The datasets generated during and/or analysed during the current study are available from the corresponding author on reasonable request.

Received: 12 April 2023; Accepted: 12 July 2023
Published online: 15 July 2023

References

1. Levin, M. Molecular bioelectricity in developmental biology: New tools and recent discoveries: Control of cell behavior and pattern formation by transmembrane potential gradients. *BioEssays* **34**, 205–217 (2012).
2. Zhao, M. Electrical fields in wound healing-An overriding signal that directs cell migration. *Semin. Cell. Dev. Biol.* **20**, 674–682 (2009).
3. Hatten, M. E. New directions in neuronal migration. *Science* **1979**(297), 1660–1663 (2002).
4. Ferrier, J., Ross, S. M., Kanehisa, J. & Aubin, J. E. Osteoclasts and osteoblasts migrate in opposite directions in response to a constant electrical field. *J. Cell Physiol.* **129**, 283–288 (1986).
5. Kim, M. S. *et al.* Homogeneity evaluation of mesenchymal stem cells based on electrotaxis analysis. *Sci. Rep.* https://doi.org/10.1038/s41598-017-09543-0 (2017).
6. Zhao, Z. *et al.* Directed migration of human bone marrow mesenchymal stem cells in a physiological direct current electric field. *Eur. Cell Mater.* **22**, 344–358 (2011).
7. Nuccitelli, R. A role for endogenous electric fields in wound healing. *Curr. Topics Dev. Biol.* **58**, 1–26 (2003).
8. Jiang, J., Li, L., He, Y. & Zhao, M. Collective cell migration: Implications for wound healing and cancer invasion. *Burns Trauma* **1**, 21 (2013).
9. Zhu, K. *et al.* Electric fields at breast cancer and cancer cell collective galvanotaxis. *Sci. Rep.* **10**, 1–11 (2020).
10. Garg, A. A. *et al.* Electromagnetic fields alter the motility of metastatic breast cancer cells. *Commun. Biol.* **2**, 1–16 (2019).
11. Sun, Y. S., Peng, S. W., Lin, K. H. & Cheng, J. Y. Electrotaxis of lung cancer cells in ordered three-dimensional scaffolds. *Biomicrofluidics* **6**, (2012).
12. Carter, S. B. Principles of cell motility: The direction of cell movement and cancer invasion. *Nature* **208**, 1183–1187 (1965).
13. Djamgoz, M., Mycielska, M., Madeja, Z., Fraser, S. P. & Korohda, W. Directional movement of rat prostate cancer cells in direct-current electric field. *J. Cell Sci.* **114**, 2697–2705 (2001).
14. Yan, X. *et al.* Lung cancer A549 cells migrate directionally in DC electric fields with polarized and activated EGFRs. *Bioelectromagnetics* **30**, 29–35 (2009).
15. Siwy, Z., Mycielska, M. E. & Djamgoz, M. B. A. Statistical and fractal analyses of rat prostate cancer cell motility in a direct current electric field: Comparison of strongly and weakly metastatic cells. *Eur. Biophys. J.* **32**, 12–21 (2003).
16. Cortese, B., Palamà, I. E., D'Amone, S. & Gigli, G. Influence of electrotaxis on cell behaviour. *Integr. Biol.* **6**, 817–830 (2014).
17. Jahanshahi, A., Schönfeld, L.-M., Lemmens, E., Hendrix, S. & Temel, Y. In vitro and in vivo neuronal electrotaxis: A potential mechanism for restoration?. *Mol. Neurobiol.* **49**, 1005–1016 (2014).
18. Guo, A. *et al.* Effects of physiological electric fields on migration of human dermal fibroblasts. *J. Investig. Dermatol.* **130**, 2320–2327 (2010).
19. Li, Y. *et al.* Effects of direct current electric fields on lung cancer cell electrotaxis in a PMMA-based microfluidic device. *Anal. Bioanal. Chem.* **409**, 2163–2178 (2017).
20. Yang, H., Charles, R.-P., Hummler, E., Baines, D. L. & Isseroff, R. R. The epithelial sodium channel mediates the directionality of galvanotaxis in human keratinocytes. *J. Cell Sci.* **126**, 1942–1951 (2013).
21. Tsai, H.-F., IJspeert, C. & Shen, A. Q. Voltage-gated ion channels mediate the electrotaxis of glioblastoma cells in a hybrid PMMA/PDMS microdevice. *APL Bioeng.* **4**, 036102 (2020).
22. Fang, K. S., Ionides, E., Oster, G., Nuccitelli, R. & Isseroff, R. R. Epidermal growth factor receptor relocalization and kinase activity are necessary for directional migration of keratinocytes in DC electric fields. *J. Cell Sci.* **112**, 1967–1978 (1999).
23. Allen, G. M., Mogilner, A. & Theriot, J. A. Electrophoresis of cellular membrane components creates the directional cue guiding keratocyte galvanotaxis. *Curr. Biol.* **23**, 560–568 (2013).
24. Huang, L., Cormie, P., Messerli, M. A. & Robinson, K. R. The involvement of Ca^{2+} and integrins in directional responses of zebrafish keratocytes to electric fields. *J. Cell Physiol.* **219**, 162–172 (2009).
25. Sato, M. J. *et al.* Input–output relationship in galvanotactic response of Dictyostelium cells. *Biosystems* **88**, 261–272 (2007).
26. Messerli, M. A. & Graham, D. M. Extracellular Electrical Fields Direct Wound Healing and Regeneration. *Biol. Bull.* **221**, 79–92 (2011).
27. Sato, M. J. *et al.* Switching direction in electric-signal-induced cell migration by cyclic guanosine monophosphate and phosphatidylinositol signaling. *Proc. Natl. Acad. Sci.* **106**, 6667–6672 (2009).
28. Nishimura, K. Y., Isseroff, R. R. & Nuccitelli, R. Human keratinocytes migrate to the negative pole in direct current electric fields comparable to those measured in mammalian wounds. *J. Cell Sci.* **109**, 199–207 (1996).
29. Rodrigues, M., Kosaric, N., Bonham, C. A. & Gurtner, G. C. Wound healing: A cellular perspective. *Physiol Rev* **99**, 665–706 (2019).
30. Erickson, C. A. & Nuccitelli, R. Embryonic fibroblast motility and orientation can be influenced by physiological electric fields. *J. Cell Biol.* **98**, 296–307 (1984).
31. Werner, S., Krieg, T. & Smola, H. Keratinocyte-fibroblast interactions in wound healing. *J. Investig. Dermatol.* **127**, 998–1008 (2007).
32. Li, J. & Lin, F. Microfluidic devices for studying chemotaxis and electrotaxis. *Trends Cell Biol.* **21**, 489–497 (2011).
33. Sun, Y.-S. Studying electrotaxis in microfluidic devices. *Sensors* **17**, 2048 (2017).
34. Halldorsson, S., Lucumi, E., Gómez-Sjöberg, R. & Fleming, R. M. T. Advantages and challenges of microfluidic cell culture in polydimethylsiloxane devices. *Biosens. Bioelectron.* **63**, 218–231 (2015).
35. Shaner, S. *et al.* Bioelectronic microfluidic wound healing: A platform for investigating direct current stimulation of injured cell collectives. *Lab Chip* https://doi.org/10.1039/D2LC01045C (2023).
36. Song, B. *et al.* Application of direct current electric fields to cells and tissues in vitro and modulation of wound electric field in vivo. *Nat. Protoc.* **2**, 1479–1489 (2007).
37. Guette-Marquet, S., Roques, C. & Bergel, A. Theoretical analysis of the electrochemical systems used for the application of direct current/voltage stimuli on cell cultures. *Bioelectrochemistry* **139**, 107737 (2021).
38. Zhang, T., Wang, L., Chen, Q. & Chen, C. Cytotoxic potential of silver nanoparticles. *Yonsei. Med. J.* **55**, 283 (2014).
39. Waters, M. D. *et al.* Toxicity of platinum (IV) salts for cells of pulmonary origin. *Environ. Health Perspect* **12**, 45–56 (1975).
40. Zajdel, T. J., Shim, G. & Cohen, D. J. Come together: On-chip bioelectric wound closure. *Biosens. Bioelectron.* **192**, 113479 (2021).

41. Zajdel, T. J., Shim, G., Wang, L., Rossello-Martinez, A. & Cohen, D. J. SCHEEPDOG: Programming electric cues to dynamically herd large-scale cell migration. *Cell Syst.* **10**, 506-514.e3 (2020).
42. Leal, J., Jedrusik, N., Shaner, S., Boehler, C. & Asplund, M. SIROF stabilized PEDOT/PSS allows biocompatible and reversible direct current stimulation capable of driving electrotaxis in cells. *Biomaterials* **275**, 120949 (2021).
43. Shaner, S. W. *et al.* Skin stimulation and recording: Moving towards metal-free electrodes. *Biosens. Bioelectron. X* **11**, 100143 (2022).
44. Leal, J., Shaner, S., Matter, L., Böhler, C. & Asplund, M. Guide to leveraging conducting polymers and hydrogels for direct current stimulation. *Adv. Mater. Interfaces* **10**, 2202041 (2023).
45. Verdes, M., Mace, K., Margetts, L. & Cartmell, S. Status and challenges of electrical stimulation use in chronic wound healing. *Curr. Opin. Biotechnol.* **75**, 102710 (2022).
46. Kirfel, G. & Herzog, V. Migration of epidermal keratinocytes: Mechanisms, regulation, and biological significance. *Protoplasma* **223**, 67–78 (2004).
47. Hong, S. H. *et al.* Stem cell passage affects directional migration of stem cells in electrotaxis. *Stem. Cell Res.* **38**, 101475 (2019).
48. Guo, A. *et al.* Effects of physiological electric fields on migration of human dermal fibroblasts. *J. Investig. Dermatol.* **130**, 2320–2327 (2010).
49. Wojtowicz, A. M. *et al.* The importance of both fibroblasts and keratinocytes in a bilayered living cellular construct used in wound healing. *Wound Repair Regen.* **22**, 246–255 (2014).
50. Iyer, K. *et al.* Keratinocyte migration in a three-dimensional in vitro wound healing model Co-cultured with fibroblasts. *Tissue Eng. Regen. Med.* **15**, 721–733 (2018).
51. Turunen, A. & Syrjänen, S. Extracellular calcium regulates keratinocyte proliferation and HPV 16 E6 RNA expression *in vitro*. *APMIS* **122**, 781–789 (2014).
52. Lei, K. F., Hsieh, S.-C., Kuo, R.-L. & Tsang, N.-M. Co-culturing cancer cells and normal cells in a biochip under electrical stimulation. *Biochip J.* **12**, 202–207 (2018).
53. Shim, G., Devenport, D. & Cohen, D. J. Overriding native cell coordination enhances external programming of collective cell migration. *Proc. Nat. Acad. Sci.* https://doi.org/10.1073/pnas.2101352118 (2021).
54. Breitwieser, G. E. Extracellular calcium as an integrator of tissue function. *Int. J. Biochem. Cell Biol.* **40**, 1467–1480 (2008).
55. Lee, S. E. & Lee, S. H. Skin barrier and calcium. *Ann. Dermatol.* **30**, 265 (2018).
56. Kee, S.-H. & Steinert, P. M. Microtubule disruption in keratinocytes induces cell-cell adhesion through activation of endogenous E-cadherin. *Mol. Biol. Cell* **12**, 1983–1993 (2001).
57. Werner, S., Krieg, T. & Smola, H. Keratinocyte-fibroblast interactions in wound healing. *J. Investig. Dermatol.* **127**, 998–1008 (2007).
58. Saltukoglu, D. *et al.* Spontaneous and electric feld-controlled front-rear polarization of human keratinocytes. *Mol. Biol. Cell* **26**, 4373–4386 (2015).
59. Trollinger, D. R., Rivkah Isseroff, R. & Nuccitelli, R. Calcium channel blockers inhibit galvanotaxis in human keratinocytes. *J. Cell Physiol.* **193**, 1–9 (2002).
60. Zhao, M. *et al.* Electrical signals control wound healing through phosphatidylinositol-3-OH kinase-γ and PTEN. *Nature* **442**, 457–460 (2006).
61. Bandyopadhyay, B. *et al.* A "traffic control" role for TGFβ3: Orchestrating dermal and epidermal cell motility during wound healing. *J. Cell Biol.* **172**, 1093–1105 (2006).
62. Kim, M. S. *et al.* Golgi polarization plays a role in the directional migration of neonatal dermal fibroblasts induced by the direct current electric fields. *Biochem. Biophys. Res. Commun.* **460**, 255–260 (2015).
63. Zhu, K. *et al.* Expression of integrins to control migration direction of electrotaxis. *FASEB J.* **33**, 9131–9141 (2019).
64. Singh, S., Young, A. & McNaught, C. E. The physiology of wound healing. *Surgery (United Kingdom)* **35**, 473–477 (2017).
65. Kloth, L. C. Electrical stimulation technologies for wound healing. *Adv. Wound Care (New Rochelle)* **3**, 81–90 (2014).
66. Sun, Y. S. Electrical stimulation for wound-healing: Simulation on the effect of electrode configurations. *Biomed. Res. Int.* https://doi.org/10.1155/2017/5289041 (2017).
67. Abedin-Do, A. *et al.* Electrical stimulation promotes the wound-healing properties of diabetic human skin fibroblasts. *J. Tissue Eng. Regen. Med.* https://doi.org/10.1002/term.3305 (2022).
68. Houghton, P. E. Electrical stimulation therapy to promote healing of chronic wounds: A review of reviews. *Chronic Wound Care Manag. Res.* **4**, 25–44 (2017).
69. Ashrafi, M., Alonso-Rasgado, T., Baguneid, M. & Bayat, A. The efficacy of electrical stimulation in experimentally induced cutaneous wounds in animals. *Vet. Dermatol.* **27**, 235-e57 (2016).
70. Isseroff, R. R. & Dahle, S. E. Electrical stimulation therapy and wound healing: Where are we now?. *Adv. Wound Care (New Rochelle)* **1**, 238–243 (2012).
71. Ud-Din, S. & Bayat, A. Electrical stimulation and cutaneous wound healing: A review of clinical evidence. *Healthcare* **2**, 445–467 (2014).
72. Karba, R., Semrov, D., Vodovnik, L., Benko, H. & Savrin, R. DC electrical stimulation for chronic wound healing enhancement. Part 1. Clinical study and determination of electrical field distribution in the numerical wound model. *Bioelectrochem. Bioenerg.* **43**, 265–280 (1997).
73. Li, M. *et al.* Toward controlled electrical stimulation for wound healing based on a precision layered skin model. *ACS Appl. Bio Mater.* https://doi.org/10.1021/acsabm.0c01190 (2020).
74. Lu, B. *et al.* Pure PEDOT:PSS hydrogels. *Nat. Commun.* **10**, 1043 (2019).
75. Tomakidi, P., Fusenig, N. E., Kohl, A. & Komposch, G. Histomorphological and biochemical differentiation capacity in organotypic co-cultures of primary gingival cells. *J. Periodontal Res.* **32**, 388–400 (1997).
76. Halbert, C. L., Demers, G. W. & Galloway, D. A. The E6 and E7 genes of human papillomavirus type 6 have weak immortalizing activity in human epithelial cells. *J. Virol.* **66**, 2125–2134 (1992).
77. Piccinini, F., Kiss, A. & Horvath, P. Cell tracker (not only) for dummies. *Bioinformatics* **32**, 955–957 (2016).

Acknowledgements

MA, JL, SS, NJ, & AS: European Research Council (ERC; 759655; SPEEDER) under the European Union's Horizon 2020 Research and Innovation program. MA: Freiburg Institute for Advanced Studies (FRIAS) and Brainlinks-BrainTools which are funded by the German Research Foundation (DFG; EXC 1086) and is currently funded by the Federal Ministry of Economics, Science and Arts of Baden Württemberg within the sustainability program for projects of the excellence initiative. We would like to thank Mrs. Ute Riede for her immeasurable help with supporting cell culture maintenance and seeding protocols, as well as Mr. Lukas Matter and Ms. Malgorzata Skorupa for their fruitful discussions about the co-culture media and MTT assay experiments.

Author contributions

J.L, S.S., and M.A. conceived the project and designed the experiments. J.L. designed and fabricated the mon.o-culture microfluidic devices and electrodes. S.S. designed and fabricated the co-culture microfluidic devices and

electrodes. N.J. and A.S. performed cell culture and seeding of devices. SS performed all F.E.A. simulations, the co-culture media experiments and metabolic assays. J.L. and S.S. performed the mono-culture and co-culture D.C. stimulation experiments, respectively. J.L. performed all cell tracking, data analysis and visualization. J.L. and S.S. equally co-wrote the manuscript. J.L. prepared Figs. 1, 2, 3 and 5. S.S. prepared Figs. 4 and 6. All authors reviewed the manuscript. M.A. provided scientific advice/guidance, funding, and supervision for all.

Funding

Open Access funding enabled and organized by Projekt DEAL.

Competing interests

The authors declare no competing interests.

Additional information

Supplementary Information The online version contains supplementary material available at https://doi.org/10.1038/s41598-023-38664-y.

Correspondence and requests for materials should be addressed to J.L. or M.A.

Reprints and permissions information is available at www.nature.com/reprints.

Publisher's note Springer Nature remains neutral with regard to jurisdictional claims in published maps and institutional affiliations.